

Contents lists available at ScienceDirect

Transportation Research Part B

journal homepage: www.elsevier.com/locate/trb





Constructing a fundamental diagram for traffic flow with automated vehicles: Methodology and demonstration

Xiaowei Shi, Xiaopeng Li

Department of Civil and Environmental Engineering, University of South Florida, Tampa, FL 33620, USA

ARTICLE INFO

Keywords:
Automated vehicle
Adaptive cruise control
Fundamental diagram
Mixed traffic

ABSTRACT

Increasingly, commercial vehicles are equipped with automated vehicle (AV) features such as adaptive cruise control systems. The AV feature can automatically control the headway between the current vehicle and the preceding vehicle in an adaptive manner. The automatic control may lead to significantly different car-following motions compared with those of human-driven vehicles, which challenges the applicability of classic traffic flow theory to emerging road traffic with AVs. To investigate the impacts of commercial AVs on traffic flow, this paper proposes a general methodology that combines both empirical experiments and theoretical models to construct a fundamental diagram (FD), i.e., the foundation for traffic flow theory for AV traffic. To demonstrate the empirical experiment settings, we collected high-resolution trajectory data with multiple commercial AVs following one another in a platoon with different headway settings. The field experiment results revealed that the traditional triangular FD structure remains applicable to describe the traffic flow characteristics of AV traffic. Further, by comparing the FDs between AVs and human-driven vehicles, it was found that although the shortest AV headway setting can significantly improve road capacity, other headway settings may decrease road capacity compared with existing human-driven-vehicle traffic. It was also found that headway settings may affect the stability of traffic flow, which has been revealed by theoretical studies but was first verified by empirical AV data. With these findings, mixed traffic flow FDs were derived by incorporating different headway settings and AV penetration rates. The method proposed in this paper, including experiment designs, data collection approaches, traffic flow characteristics analyses, and mixed traffic flow FD construction approaches, can serve as a methodological foundation for studying future mixed traffic flow features with uncertain and evolving AV technologies.

1. Introduction

Fundamental diagram (FD) describes a well-defined relation curve for traffic flow rates and density in steady traffic states (Daganzo, 1997; Greenberg, 1959; Newell, 1961). The FD is critical to study traffic flow characteristics and dynamics across various spatial scales with analysis, modeling, and simulation methods (Daganzo and Geroliminis, 2008; Geroliminis and Sun, 2011a; Knoop and Hoogendoorn, 2013; Zhang et al., 2018). A series of studies was conducted on models, properties, and estimation methods of FD (Delis et al., 2018; Nikolos et al., 2015; Qu et al., 2017). For example, Qu et al. (2015) proposed a novel calibration approach for

E-mail addresses: xiaoweishi@usf.edu (X. Shi), xiaopengli@usf.edu (X. Li).

^{*} Corresponding author.

single-regime FD models by using a weighted least squares method that can address the sample selection bias problem in existing single-regime models. Tian et al. (2012) studied the properties of the FD and synchronized flow by incorporating the anticipation rule into the Nagel–Schreckenberg model (Nagel and Schreckenberg, 1992). They found that the proposed model observed the same spatiotemporal dynamics as many of the more complex models. Wang et al. (2013) presented a speed-density model that aims to incorporate stochasticity in FD. Knoop and Daamen (2017) proposed a two-stage method for enhancing the fitting performance of FD with loop detector data. Seo et al. (2019) studied the estimation of the FD with trajectory data collected by probe vehicles. Overall, the FD is a fundamental concept of traffic flow theory and has been applied to a wide variety of research problems and engineering applications.

Recently manufactured commercial vehicles are increasingly equipped with automated driving features. For example, the adaptive cruise control (ACC) system, arguably the most common automated vehicle (AV) driving feature, is available on many new models of commercial vehicles in recent years. The ACC system is composed of a series of onboard sensors (e.g., millimeter-wave radars) and computing and control units (Wang et al., 2019). The ACC system automatically maintains a safe headway between the subject AV and the lead vehicle by dynamically controlling the AV speed with real-time sensor information. Note that such commercial AVs are controlled by exact, prescriptive, and fast-responding computer-mechanical dynamic models, whereas human-driven vehicles often exhibit uncertain, unpredictable, and slow-responding driving behaviors. Therefore, commercial AVs may fundamentally alter traffic flow characteristics as their market penetration increases rapidly (Auld et al., 2018; J. 2017; Soteropoulos et al., 2019). It was recorded that the market penetration of commercial AVs with ACC operating on highway systems will increase from 2% in 2015 to over 10% in 2025 (Calvert et al., 2017). It is predicted that half of vehicles sold and 40% of vehicles on the road will be equipped with automated driving features by the 2040s.

Existing studies on macroscopic AV traffic characteristics focused on the impacts of AVs on traffic flow capacity (Arnaout and Arnaout, 2014; Ghiasi et al., 2019; A. 2017; Liu et al., 2018; Shladover et al., 2012; Van Arem et al., 2006). For example, Arnaout and Arnaout (2014) proposed an agent-based microscopic simulation model to estimate the impacts of AVs on the capacity of a multi-lane highway system. Shladover et al. (2012) examined the effect on highway capacity of varying AV market penetrations by microscopic simulation methods. Despite the successes of these pioneering studies, existing capacity analysis studies mainly focused on the highest throughput, whereas the FD concerns the full spectrum of traffic flow characteristics (e.g., steady state) across all density values (Zhou and Zhu, 2020). Further, most of these studies validated their findings using a simulation-based approach relying on assumptions of AV controls (e.g., extremely short headway and precise vehicle control), which may not be consistent with the behaviors of commercial AVs (Gunter et al., 2019; Milanes et al., 2014; Shi and Li, 2020).

Modeling the full FD for a pure AV or mixed human-driven vehicle and AV traffic is relatively scarce in the literature (Baskar et al., 2009; Bose and Ioannou, 2003; Levin and Boyles, 2016; Yao et al., 2019; Ye and Yamamoto, 2018; Zhou and Zhu, 2020). To generate optimal routing solutions for intelligent vehicle highway systems, Baskar et al. (2009) studied the FD of pure AV traffic by fixing the AV following headway to a small value (i.e., 0.5 s). Bose and Ioannou (2003) analyzed the FD of mixed traffic from pure human-driven vehicle traffic to pure AV traffic by assuming that the AVs have a smaller headway than human-driven vehicles due to the use of sensors and actuators. Levin and Boyles (2016) investigated the mixed traffic FD of AVs and human-driven vehicles by proposing a multiclass cell transmission model. Yao et al. (2019) studied the mixed traffic FD with different AV penetration rates and analyzed the influence factors of the FD. Ye and Yamamoto (2018) proposed a two-lane cellular automaton model to study the mixed traffic FD with different AV penetration rates. The most recent study on the modeling of FD for mixed traffic was Zhou and Zhu (2020). Changes of AV penetration rate and platooning intensity were considered when generating the FD. Despite these successes, the existing studies modeled the FD with simple analysis or pure simulation with very optimistic assumptions of AV controls, which may overestimate the actual performance of existing commercial AVs. Such overestimations or biases from theoretical studies alone may lead to sub-optimal operations (e.g., ineffective platooning operations) and planning (e.g., future roads not reaching expected high capacity, thus causing transportation system breakdowns) decisions in practice when facing emerging AV traffic.

To effectively support informed decisions in the AV traffic era, there is a need to build an FD with real-world AV data. As vehicle motion characteristics of the AV may vary and evolve as the technology develops in the near future, it is imperative to develop a general approach for modeling traffic flow characteristics for the evolving AV traffic.

To this end, this paper aims to make the following contributions to the literature:

- (1) This paper proposes a general method for constructing the FD for AV traffic, integrating empirical experiments and data analytics. The proposed method, including experiment designs, data collection approaches, traffic flow characteristics analyses, and mixed traffic flow FD construction approaches, can be easily adopted for future traffic despite technology evolutions.
- (2) To the best of the authors' knowledge, this paper is the first research that constructs the FD for AV traffic with empirical data. Some results obtained by this paper were found that are consistent with those predicted by theoretical studies, including that (i) the greater the free flow velocity is, the greater the traffic capacity will be (Yao et al., 2019); and (ii) the smaller the following headway is, the larger the capacity is (Levin and Boyles, 2016; Yao et al., 2019; Ye and Yamamoto, 2018).

Although some results are inconsistent with those predicted by the theoretical studies, including (i) AV technologies can significantly improve road capacity (Baskar et al., 2009; Bose and Ioannou, 2003) and (ii) the greater the AV penetration rate is, the greater the traffic capacity will be (Levin and Boyles, 2016; Yao et al., 2019; Ye and Yamamoto, 2018; Zhou and Zhu, 2020). Based on our findings, only the shortest AV headway setting can significantly improve road capacity, and some other headway settings may even reduce road capacity. Thus, as the AV penetration rate increases, the traffic capacity variation trend is unclear, which is dependent on the enabled AV headway settings.

This paper also reveals findings that have not been reported in the AV FD literature to date, including (i) the traditional triangular FD structure remains valid to describe AV traffic stationary states, and (ii) AV headway settings may affect the stability of traffic flow. Note that although a series of microscopic studies have verified that AV headway settings will affect traffic stability (Gunter et al., 2019; Shi and Li, 2020), none reveal this relationship on the FD. This paper fulfills this research gap.

Following these findings, managerial insights into effective AV traffic management are drawn: (i) to maximize the utilization of road infrastructures in peak hours, policies could be made to encourage the use of shorter headway settings to mitigate congestions, and (ii) to stabilize traffic oscillation and thus improve the driving experience of passengers, when traffic capacity is sufficient (e.g., off-peak hours), the use of longer headway settings may be encouraged for a more stable driving experience.

The rest of this paper is organized as follows. Section 2 presents the methods to extract traffic flow characteristics from vehicle trajectory datasets. Section 3 proposes the method for designing and conducting corresponding field experiments to collect such trajectory data. Section 4 shows the datasets analyzed in this paper. Results are discussed in Section 5. Section 6 describes the mixed traffic flow FD construction approach. Section 7 summarizes the paper and identifies future research directions.

2. Methods for measuring traffic flow characteristics

This section presents two methods from the macroscopic and microscopic perspectives to measure traffic flow characteristics (i.e., density, flow rate, and speed). The estimated traffic flow characteristics may be used to construct the corresponding FD.

2.1. Macroscopic method

When a stream of trajectory data is available, we can study traffic flow characteristics by the macroscopic method proposed by Edie (1963), known as Edie's generalized definition of traffic variables. In this paper, a vehicle trajectory means the curve of the location of a certain reference point on a vehicle (e.g., mid-point of front bumper) over time. This method deals with a n-vehicle platoon inside an arbitrary time-space region A. Density k, flow rate q, and speed v in region A can be calculated by (1)-(3).

$$k = \sum_{i=1}^{n} t_i / |A|, \tag{1}$$

$$q = \sum_{i=1}^{n} x_i / |A|, \tag{2}$$

$$v = q / k = \sum_{i=1}^{n} x_i / t_i, \tag{3}$$

where |A| denotes the area size of region A and t_i , x_i are the ith vehicle travel time and distance traveled inside A, respectively, as illustrated in Fig. 1.

In this paper, A is set as a parallelogram region constructed with two sides parallel to the shockwave speed of w and the other two parallel to trajectories, as shown in Fig. 2. In this way, one maximizes the chances of having stationary conditions inside the region (Laval, 2011).

Such trajectory data in a long platoon may not always be available due to limited experiment resources. When a platoon is relatively

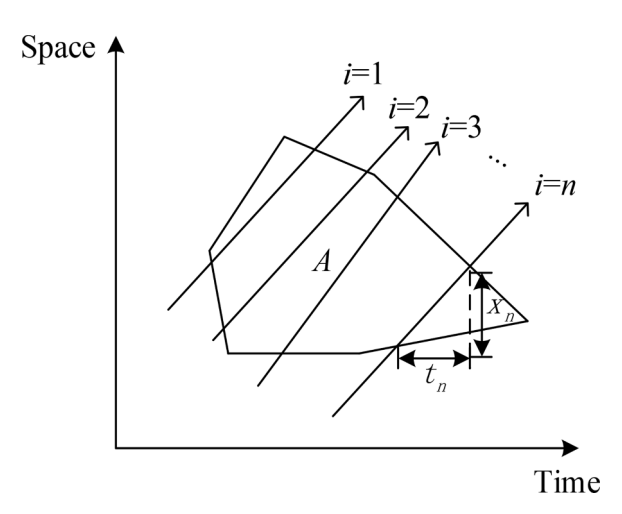


Fig. 1. Illustration of parameters for traffic flow characteristics calculations.

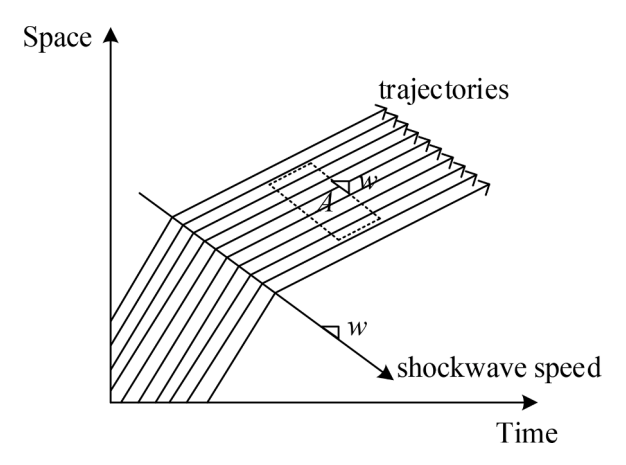


Fig. 2. Illustration of generated parallelogram region for platoon trajectories.

short (e.g., only a couple of vehicles), it would be difficult to apply the above macroscopic method to construct traffic flow characteristics accurately. To address this issue, we propose a microscopic method to measure the traffic flow characteristics with only two consecutive vehicle trajectories. Note that the FD describes the relationship of the flow rate and density at steady states. Thus, to maximize the possibilities that the calculated flow rate and density can describe steady-state characteristics, only trajectory segments that the two vehicles have relatively constant speed are selected for the following calculations. The microscopic method is described as follows.

For two consecutive trajectories, we consider a time-space region B (as shown in Fig. 3). Note that the lower and upper sides of the region are the corresponding segments of the two trajectories within the same time window t. Density k, flow rate q, and speed v for region B can be calculated by (4)-(6).

2.2. Microscopic method

$$v = x/t, (4)$$

$$k = t/|B|), (5)$$

$$q = kv = x/|B|,\tag{6}$$

where t, x denote the following vehicle travel time and distance traveled inside B, and |B| is the area of region B. What must be emphasized is that the proposed microscopic method arguably is the most efficient way to study the characteristics of traffic flow without much loss of generality when experiment resources are limited; otherwise, the macroscopic method is preferred.

With these two methods, by successively moving the region *A* or *B* throughout the study trajectories, the traffic flow characteristics (e.g., density, flow rate, and speed) are obtained. Then, the FD can be obtained by fitting the characteristic data points in the flow-density diagram.

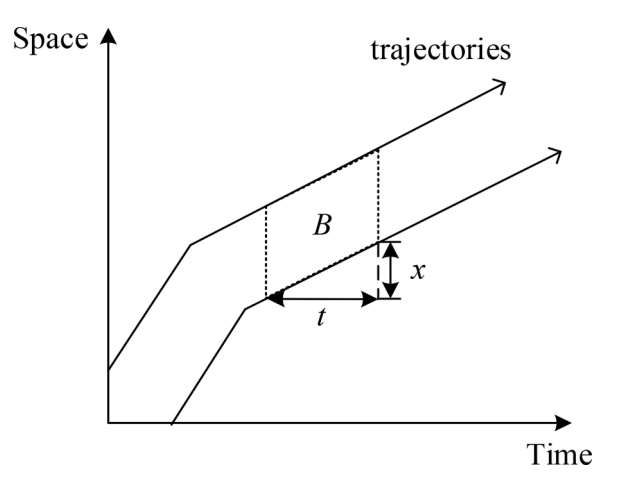


Fig. 3. Illustration of generated region for vehicle following trajectories.

3. Experiment design for data collection

This section provides a general experiment design framework for collecting the AV trajectory data. Our experiment design is introduced as an example of the proposed method, including experiment vehicle fleet, data collection devices, and experiment planning.

3.1. Experiment design frameworks

The experiment vehicle fleet, data collection devices, and experiment planning are crucial to conducting AV trajectory data collection experiments. To study traffic flow characteristics at different speed ranges, the lead vehicle needs to follow a trajectory with specific speed changes; thus, the speed profile of the lead vehicle is somehow controlled. One convenient approach is to use a vehicle with a cruise control system that can automatically adjust its speed according to a specific input speed profile. It is better if one can use an onboard computer or a laptop to input the speed change commands to avoid the delay caused by human drivers.

The following distance between every two consecutive vehicles is essential to study traffic flow characteristics. Here, we propose two approaches to capture the following distances. The first approach is to use a global positioning system (GPS) receiver to obtain the real-time absolute position of each vehicle, and the second approach is to use a distance radar to measure the real-time relative distance between every two consecutive vehicles (Wang et al., 2019). Note that the GPS-based approach is generally more economical and easier to configure than the radar-based approach. The GPS devices usually have magnetic pads and can be mounted on vehicles easily without any permanent damage to the vehicle body. However, of note is that the accuracy of the GPS-based approach may be more susceptible to environmental factors such as weather and building density. Therefore, an appropriate experiment site is also crucial to the data collection using the GPS-based approach.

As an FD describes the flow-density relation under various traffic scenarios (i.e., corresponding to different equilibrium speeds), the experiment planning should simulate as many traffic scenarios as possible to cover the whole flow range—the speed profiles of the lead vehicle should include as many speed ranges as possible.

3.2. Experiment design example

This section proposes an experiment design conducted on a four-lane segment SR-56 in Florida, as shown in Fig. 4, which illustrates the proposed experiment design method. Note that the sparse traffic and buildings of the segment provide an ideal experiment site to collect the data.

Experiment vehicle fleet

The vehicles employed in the experiments included two commercial AVs and one regular vehicle with a cruise control (CC) system. The AVs were Lincoln MKZs for model years 2016 and 2017, both of which had four different following headway settings, such as 1 to 4 (i.e., headways from short to long). The regular (CC) vehicle was a 2015 Audi Q7, and the speed of the vehicle could be manually controlled by the input button of the CC system.

Data collection devices

Real-time GPS positions and speeds of the experiment vehicles were collected at a sampling rate up to 10 Hz by high-accuracy U-blox C099-F9P GPS receivers with the antenna affixed to the rear bumper on each vehicle. Preliminary testing indicated that the GPS receivers have a mean position accuracy of 0.26 m and a speed accuracy of 0.089 m/s. Thus, the real-time vehicle-following spacing between every two consecutive vehicles could be obtained by the distance between the GPS positions of the two vehicles minus the following vehicle length.

Experiment planning

In the platooning experiments, the CC vehicle served as the lead vehicle, and the Lincoln MKZ 2016 and 2017 were the second and



Fig. 4. Segment of SR-56 in Florida. (Source: Google maps).

third vehicles. These vehicles followed one another and formed a vehicle platoon. Note that the AVs can also serve as CC vehicles if the radar systems of the AVs do not detect any preceding vehicles at the same lane. The experiments were conducted at late night with less traffic so the AVs could also maintain the desired speed by inputting the speed into the ACC systems. With this, in the car-following experiments, the Lincoln MKZ 2016 served as the lead vehicle and the Lincoln MKZ 2017 enabled the ACC function following the lead vehicle. Note that both sets of experiments were conducted in a single lane.

Fifteen speed profiles for each headway setting (i.e., headway setting 1 to 4) were executed by the lead vehicle to study the behavior of the commercial AVs under different speed ranges and headway settings. The first five speed profiles were the high-speed range tests (45–55 mph), the next five speed profiles were the mid-speed range tests (35–45 mph), and the remainder were the low-speed range tests (25–35 mph). Each speed profile was conducted twice for cross validation before proceeding to the next speed profile, resulting in 60 tests for each headway setting, including 30 for the platooning experiment and 30 for the car-following experiment (10 for each speed range). Each test included 3 phases with an identical duration (30 s). Each test started when all vehicles reached a given initial cruise speed (e.g., 55 mph for high-speed range tests). In the first phase (i.e., first 30 s), the lead vehicle cruised at the initial speed. In the second phase (i.e., 30–60 s), the lead vehicle changed its speed to a desired lower speed (i.e., 53 mph for test 1) and then cruised at the desired speed for the rest of the time in this phase. In the third phase (60–90 s), the lead vehicle changed its speed back to the initial speed (i.e., 55 mph) and then cruised at the initial speed until the end of this phase. The detailed test plan for the platooning experiment of headway setting 1 (tests 1–30) is shown in TABLE I, where v_I is the initial speed and v_T is the target speed of the lead vehicle. The carfollowing experiment (tests 31–60) had the same test settings as the platooning experiment.

Note that the specified lead vehicle's speed profile was implemented by setting the lead vehicle's CC/ACC to the desired speed. When changing speed, the manual input button was used to adjust the speed of the lead vehicle to the newly desired speed. The following vehicle(s) followed the preceding vehicle in the ACC mode with a sufficiently high target speed (e.g., 80 mph) that did not constrain the acceleration or speed of the vehicle(s). With this, 240 tests (60 for each headway setting) were conducted, and the recorded trajectory length was about 250 miles in total.

4. Dataset

Three sets of data were investigated in this study. Datasets 1 and 2 are the trajectory data of AVs, and dataset 3 is the trajectory data of human-driven vehicles, which serves as a benchmark of the studied FD of the AVs. A detailed introduction to each dataset follows.

4.1. Dataset 1

The first dataset includes three-vehicle platoon trajectory data and two-vehicle car-following data, collected by the proposed data collection method. The dataset can be found at https://github.com/CATS-Lab-USF.

4.2. Dataset 2

The second dataset was generously shared by Gunter et al. (2020). Two types of trajectory data were included—a five-vehicle platoon trajectory dataset (including one lead autonomous test vehicle for which control commands can be input from onboard computers and four following commercial AVs), and a two-vehicle car-following trajectory dataset (including one lead CC vehicle and one following commercial AV). The following AVs in the experiments had the same ACC systems with two headway settings, e.g., short and long headway settings. Similarly, the experiments were conducted at two-speed ranges, high (65–75 mph) and low (35–55 mph) speed ranges. In the experiments, the lead vehicle executed a specific pre-defined speed profile (including quick acceleration and deceleration) and the following vehicles (four or one commercial AVs) drove in a single lane followed the lead vehicle by controlling the onboard ACC system. Due to limited experiment resources, the platoon trajectory data were relatively short, so we could not accurately construct traffic flow characteristics using the macroscopic method. Therefore, the car-following trajectory dataset was processed with the proposed microscopic method instead.

Table ITest plan for platooning experiment of headway setting 1.

Test number	ν ₁ (mph)	v_T (mph)	Test number	v_I (mph)	v_T (mph)	Test number	v_I (mph)	v_T (mph)
1	55	53	11	45	43	21	35	33
2	55	53	12	45	43	22	35	33
3	55	51	13	45	41	23	35	31
4	55	51	14	45	41	24	35	31
5	55	49	15	45	39	25	35	29
6	55	49	16	45	39	26	35	29
7	55	47	17	45	37	27	35	27
8	55	47	18	45	37	28	35	27
9	55	45	19	45	35	29	35	25
10	55	45	20	45	35	30	35	25

4.3. Dataset 3

The third dataset was a set of trajectory data of human-driven vehicles in a specified segment of I-75 in Florida, which served as a benchmark to the studied traffic flow characteristics of the commercial AVs. Videos of human-driven vehicle trajectories were taken via helicopter. Then, the trajectory data were extracted from the videos by the video processing method proposed by Zhao et al. (2021). Trajectory data can be found at https://github.com/CATS-Lab-USF and will also be available on the official website of the Federal Highway Administration soon.

5. Experiment results and discussions

3500

We first studied the characteristics of traffic flow for each dataset by using the methods proposed in Section 2. Based on the trends of the characteristics, the triangular FD was adopted to interpret the relationships among the traffic flow characteristics. Then, comparisons of traffic flow characteristics between the AVs and human-driven vehicles were conducted to provide insights into the impacts of AVs on traffic flow.

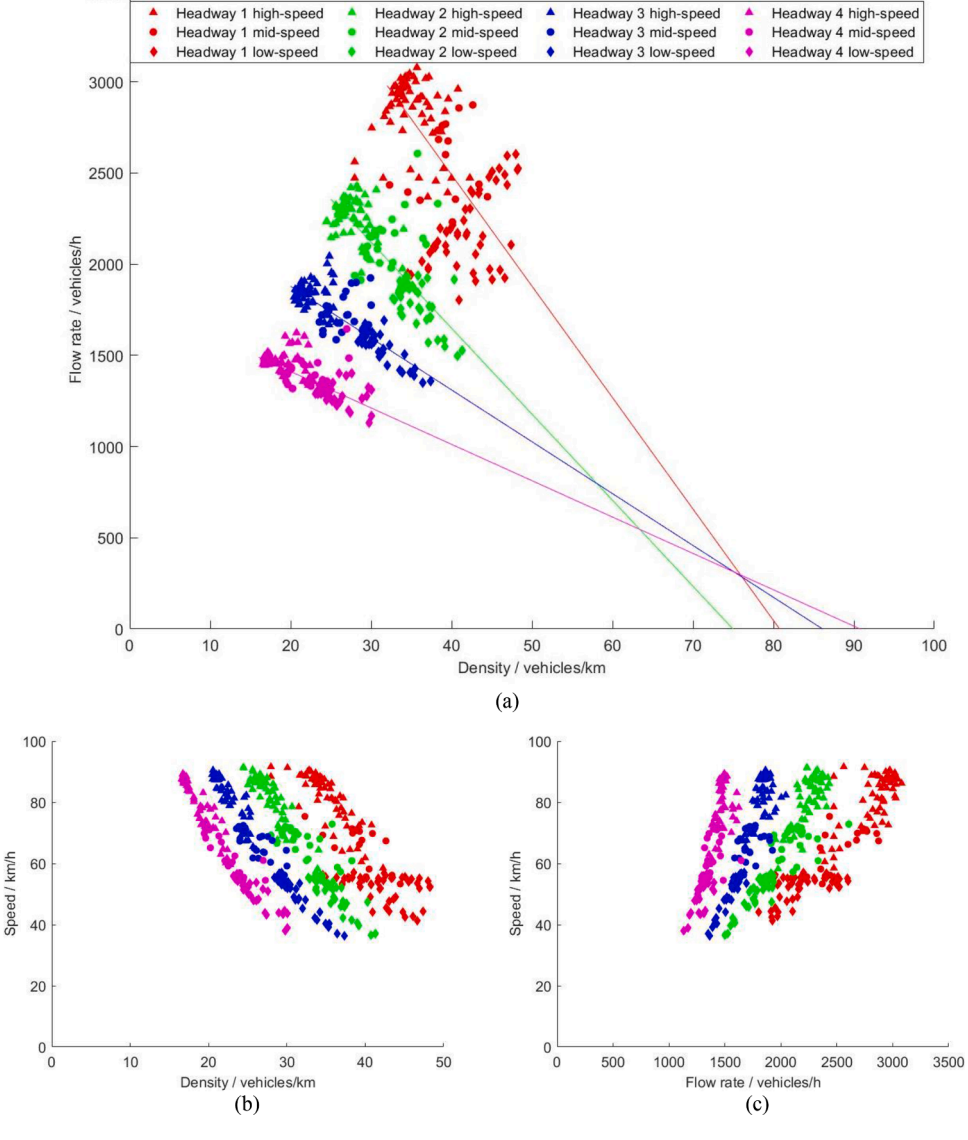


Fig. 5. Density-flow rate, density-speed, flow rate-speed scatter plots for Dataset 1.

5.1. Experiment results and analyses

5.1.1. Dataset 1

Fig. 5(a)–(c) shows scatter plots of traffic flow characteristics generated by dataset 1. To differentiate the data from different experiment settings, the points from high-speed, mid-speed, and low-speed tests are marked with triangles, circles, and diamonds, respectively. The points of headway settings 1–4 are red, green, blue, and pink, respectively.

Fig. 5(a) plots the flow rates over the density of the studied dataset. It can be seen that all data points are in the congested regime of the FD. This is because all data points were associated with the car-following mode, whereas the free-flow regime of the FD (left side of congestion) corresponds to all AVs cruising at free-flow speed without downstream impedance. Thus, even without data points, the free-flow regime can be easily estimated with a straight line from the origin point with a slope of the given free-flow speed (often depending on the road speed limit). Therefore, in engineering applications, the free-flow regime is often trivial, and the congestion regime is often the focus. Thus, we focused on the congestion regime in the following analysis. Next, it can be found in Fig. 5(a) that as density increases, the flow rate exhibits a decreasing trend, and the longer the headway is, the lower the flow rate is, and the slower the decreasing slope is. This indicates that the road capacity (i.e., maximum flow rate across all density) decreases as the AV headway setting increases. For the longest headway setting (#4), the road capacity is only around 1500 vehicles/hour, which is about half of that for the shortest headway setting, i.e., around 2900 vehicles/hour. This empirical finding is informative to future road traffic management by relevant stakeholders. For example, to maximize the utilization of road infrastructures in peak hours, policies could be made to encourage the use of shorter headway settings to mitigate congestion.

The classic triangular FD has many merits in traffic flow studies, such as the fixed free flow rate and shock wave speed. Thus, this structure indicates that the flow-density relationship in the congestion regime can be captured by a linear function. We fitted a linear function to the points in Fig. 5(a) of each headway setting. The fitting parameters of the linear function for each headway setting, including flow rate capacity, shock wave speed, jam density, and fitness results such as the adjusted R^2 , are shown in TABLE II. It was found that the fitted straight lines had relatively good fitness, indicating that the triangular FD structure remains applicable to describe the characteristics of AV traffic.

Note that the adjusted R^2 values of headways 3 and 4 are better than those of headways 1 and 2, which indicates that a longer headway setting tends to yield more steady traffic. This indication can also be verified by the widespread data points of headways 3 and 4 in Fig. 5(a). This result provides empirical support to the trade-off between traffic stability and AV headway settings—a longer AV headway, though decreasing traffic capacity, may help stabilize traffic oscillation. The implication to policymaking is that when traffic capacity is sufficient (e.g., off-peak hours), the use of longer headway settings may be encouraged. Refer to Li (2020) and Shi and Li (2020) for string stability analysis with different headway settings.

Further, we observed that the fitted straight lines intersect with the horizontal axis (i.e., density axis) in Fig. 5(a). Each intersection indicates the jam density for the corresponding headway setting—once the traffic flow stops completely, how many vehicles can be accommodated by the road in one kilometer. The results show that the jam density values across different headway settings are approximately identical, at around 85 vehicles/km.

To provide different perspectives of the traffic flow characteristics, Fig. 5(b) and (c) plot the density-speed and flow rate-speed relationships from the observed data points, respectively. In the density-speed figure (Fig. 5(b)), as density increases, speed exhibits a decreasing trend. In the flow rate-speed figure (Fig. 5(c)), as the flow rate increases, speed exhibits an increasing trend. Further, the data points across different headway settings seem to all converge at the origin with proper extrapolation, which verifies that when the speed drops to 0, the flow rate is also 0. These trends are the same as those described by the congestion regime of the triangular FD, which further validates the suitability of the triangular FD structure in analyzing these data.

5.1.2. Dataset 2

Fig. 6(a)-(c) show the scatter plots of traffic flow characteristics generated by dataset 2. Similarly, all data points are in the congested regime of FD. Also, significant correlations among the traffic density, flow rate, and speed are shown in the figure. For consistency, the points of the long headway setting are pink and those of the short headway setting are red. The points from high-speed tests are marked with triangles and those from low-speed tests are marked with circles.

Fig. 6(a) plots the flow rates over the density of dataset 2. It was found that as density increases, the flow rate exhibits a decreasing trend, and the long headway setting has lower values of the flow rate and decreasing slope than the short headway setting. The road capacity for the short and long headway settings of dataset 2 is approximately 2550 and 1480 vehicles/hour, respectively.

By fitting a linear function to the data points in Fig. 6(a) of each headway setting, the fitting parameters of the linear function of

Table IIFitting parameters of triangular FDs.

Dataset	Headway setting	Road capacity (vehicles/h)	Shock wave speed (km/h)	Jam density (vehicles/km)	Adjusted R ²
1	1	2900	61.1	80.77	0.50
	2	2250	47.2	74.96	0.64
	3	1850	28.4	86.11	0.75
	4	1500	20.0	90.77	0.67
2	Short	2550	64.4	62.00	0.10
	Long	1480	30.0	60.91	0.22
3 (Human-driven)		2000	30.5	94.40	0.79

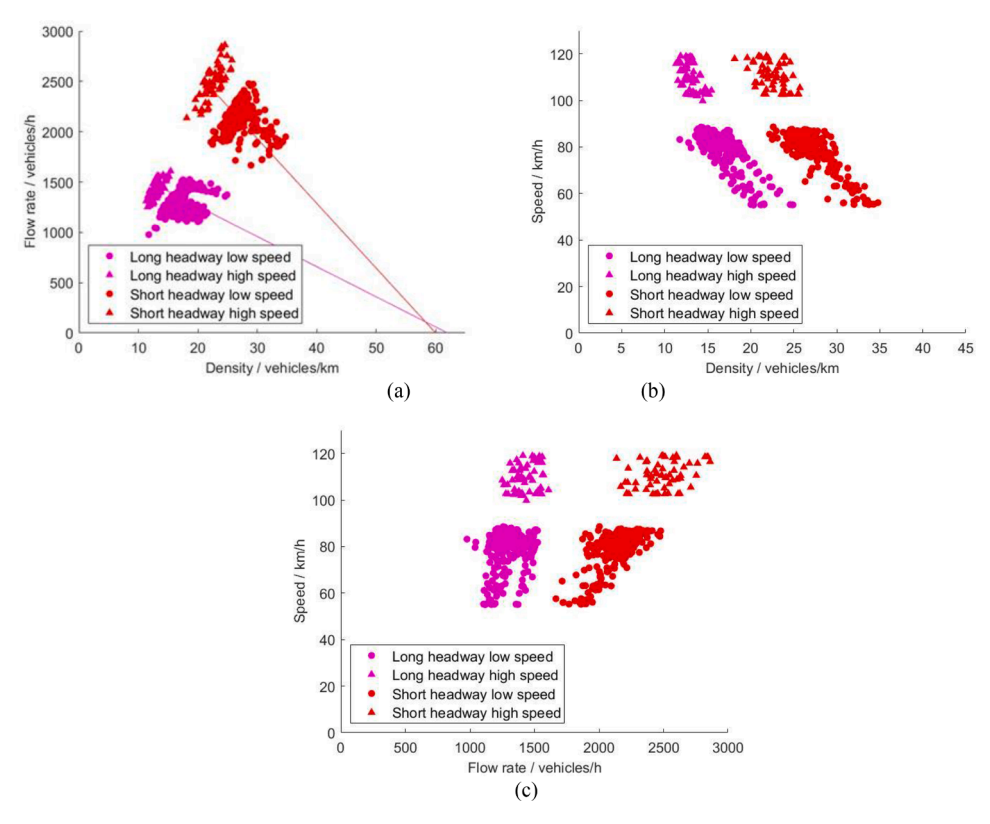


Fig. 6. Density-flow rate, density-speed, flow rate-speed scatter plots of Dataset 2.

dataset 2 are shown in TABLE II. The values of adjusted R^2 shown in TABLE II, indicating that the model fitness is significantly different from Datasets 1 and 2. Although the data points of headways 1 and 2 in dataset 1 are dispersed, as shown in Fig. 5(a), the average value of adjusted R^2 of dataset 1 over the four headway settings is 0.64. However, the average value of adjusted R^2 of dataset 2 over the two headway settings is 0.16. The main reason for this difference may be because of the pertinent experiment design described in Section 3. That is, the experiment design proposed herein includes more traffic flow steady states than that proposed in Gunter et al. (2020). Therefore, the data points of dataset 1 shown in Fig. 5 are more aggregated than those of dataset 2 shown in Fig. 6. Moreover, the jam density values across different headway settings for dataset 2 are approximately identical, around 60 vehicles/km.

Fig. 6(b) and (c) plot the density-speed and flow rate-speed relationships of dataset 2, respectively. The relationships follow the same trends as those of dataset 1. In the density-speed figure (Fig. 6(b)), as the density increases, the speed exhibits a decreasing trend. In the flow rate-speed figure (Fig. 6(c)), as the flow rate increases, the speed exhibits an increasing trend.

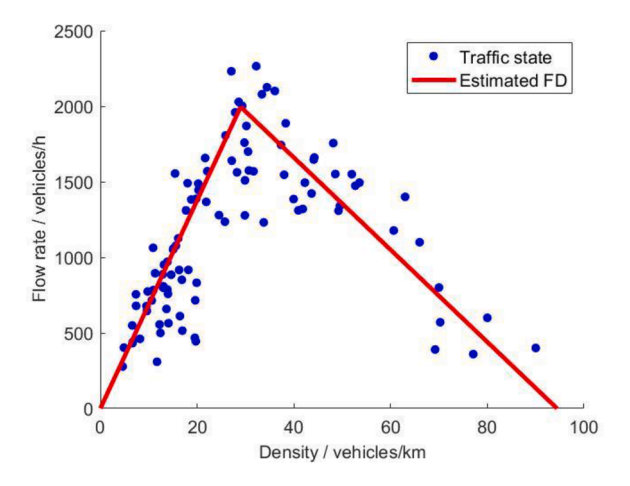


Fig. 7. FD plots of dataset 3.

5.1.3. Dataset 3

Fig. 7 plots the flow rates over the density of dataset 3 (i.e., human-driven data). Due to the available data points in the free-flow regime, both the free-flow and congested regimes can be found in Fig. 7. We fit a linear function to the data points at the congested regime in Fig. 7 and the fitting parameters of the linear function is shown in TABLE II. Note that the traffic flow FD of human-driven vehicles has been well investigated by existing studies (Gayah et al., 2014; Geroliminis and Sun, 2011b; Knoop and Hoogendoorn, 2013), and the obtained fitting parameters of dataset 3 are consistent with the previous studies' findings. The estimated free-flow speed of the dataset is about 70 km/h. The value of the adjusted R^2 of the fitness is 0.79, indicating a relatively good fitness of the triangular FD.

5.2. Comparisons and discussions

The above sections present the traffic flow characteristics and the FDs of the three datasets. In this section, traffic flow characteristics among the three datasets are compared and discussed to draw insights into the impacts of AVs on traffic flow.

Compared the results of the AV datasets (datasets 1 and 2) in TABLE II, the estimated road capacity is almost consistent over the two datasets. The maximum and minimum road capacity obtained from dataset 2 is 2550 vehicles/hour and 1480 vehicles/hour, respectively. These values are on the same order of magnitude with the maximum (2900 vehicles/hour) and minimum (1500 vehicles/hour) road capacity obtained from dataset 1, whereas the actual values are slightly smaller than those in dataset 1. The consistency indicates that different automakers may follow similar general principles in designing ACC control, which enables our FD method to generally apply across different vehicle technologies. This slight difference may be due to different ACC configurations and vehicle dynamics between different vehicle vendors and other heterogeneous exogenous factors while conducting the experiments (e.g., speed limit, road conditions, etc.).

TABLE II shows the fitting parameters across the six headway settings of the two AV datasets (i.e., four headway settings of dataset 1 and two headway settings of dataset 2). As shown, as the headway increases in both datasets, road capacity decreases and the shockwave speed decreases, whereas the jam density does not change much. This indicates that different headway settings will mainly affect traffic throughput when traffic is mildly congested but may have fewer impacts in highly congested traffic. We also see that the jam density value of dataset 2 (60 veh/km) is smaller than that of dataset 1 (85 veh/km). One possible explanation is that the ACC system design in dataset 2 is more conservative than the ACC system in dataset 1 when traffic is highly congested. Thus, when traffic flow stops completely, a smaller number of vehicles can be accommodated by the road in one kilometer with the ACC system in dataset 2 compared with that in dataset 1.

Overall, in both AV datasets, the impacts of AVs on traffic flow are related to the enabled headway settings—a shorter headway setting improves road capacity. Further, the values of the minimum and maximum capacity across different AV vendors are consistent despite some minor discrepancies. This finding verifies the potential transferability of the proposed AV FD modeling framework across different AV technologies for engineering applications that may tolerate certain errors. However, if more accurate measures are needed, the heterogeneity of AV traffic flow may need to be taken into consideration in future studies.

Note that the estimated parameters of the FDs are different across the different datasets, as shown in TABLE II. The road capacity of the human-driven vehicles is about 2000 veh/hour, which is between the highest capacity (with the shortest headway) and the lowest capacity (with the longest headway) of AV datasets 1 and 2. This result draws the following insights into existing commercial AV following designs. First, it suggests that vehicle vendors may design AV following algorithms in accordance with the traffic flow characteristics of human-driven vehicles. AV headway settings are comparable to the average following headway of human drivers while allowing some variation range to suit preferences from heterogeneous individual drivers. Second, the merits of AVs proposed by previous studies that AV technologies can significantly improve the road capacity may be too optimistic. Based on the estimated results of this study, only the shortest headway setting can significantly improve road capacity (from 2000 veh/hour to 2900 or 2550 veh/hour dependent on the result of which dataset is adopted), whereas some other headway settings may even reduce the road capacity.

Further, it is worth mentioning that although we found that a shorter headway setting improves road capacity, safety concerns will be raised once the headway setting is too short (Robbins et al., 2018). Also, headway settings may affect the stability of the traffic flow. Once the enabled headway setting is too short, traffic flow becomes less stable, and road capacity may drop (Li, 2020; Shi and Li, 2020).

6. Mixed traffic flow fundamental diagram

As the AV feature (ACC system) is equipped on only a relatively small subset of vehicles currently, pure AV traffic flow is still far from reality. Instead, it is likely that mixed traffic flow containing both AVs and human-driven vehicles will dominate road traffic for a long time. Investigations of mixed traffic flow characteristics are essential for the analysis, modeling, and simulation of future traffic as AV penetration rates increase. Extended from the analytical methods for mixed traffic flow characteristics proposed by A. Ghiasi et al. (2017) and Qian et al. (2017), we propose a general and parsimonious method to formulate a mixed traffic FD function, i.e., mixed traffic flow rate over density, based on the above pure AV/human-driven vehicle FDs in the following analysis.

Consider a set of different vehicle types, denoted by \mathcal{J} , e.g., including human-driven vehicles, AVs with headway settings 1, 2, 3 and 4, etc. Note that if platooning with connected vehicles are considered, vehicle following behaviors may depend not only on the subject vehicle but also the preceding vehicle (e.g., an AV following a human-driven vehicle may have different following behaviors as opposed to an AV following another AV that is platooned with a shorter headway; see A. Ghiasi et al. (2017)). Assume that the pure traffic with type-j vehicles follows the following FD equation:

$$q_{j}(k) = \begin{cases} \overline{v}k, & k \in \left[0, q_{j}^{0}/(\overline{v} + w_{j})\right] \\ -w_{j}k + q_{j}^{0}, & k \in \left[q_{j}^{0}/(\overline{v} + w_{j}), q_{j}^{0}/w_{j}\right] \end{cases}$$

$$(7)$$

where \bar{v} is the speed limit of the studied road (we assume all vehicle types share the same speed limit on the same road), $-w_j$ is the FD slope of the congestion regime (or the corresponding backward shockwave speed), and q_j^0 is the intercept of the congested-regime FD branch and the flow rate axis. These parameters are illustrated in Fig. 8. Note that each regressed curve in Fig. 5(a), Fig. 6(a), and Fig. 7 is such a pure traffic FD (or the congested regime of it).

In the investigated mixed traffic, let α_i denote the penetration rate of type-j vehicles $\forall j \in \mathscr{J}$, and let k denote the total mixed traffic density. Then $k_j = k\alpha_j$ is the density of type-j vehicles in mixed traffic. When $\sum\limits_{j \in \mathscr{J}} (\overline{v} + w_j)k_j/q_j^0 \leq 1$ (or $k \leq 1/\left(\sum\limits_{j \in \mathscr{J}} (\overline{v} + w_j)\alpha_j/q_j^0\right)$, the occupancy for each type of vehicles is sufficiently low to maintain their vehicle speed at speed limit \overline{v} , and the mixed traffic's state is in the free-flow regime. In this case, the mixed traffic flow q(k) is simply identical to $\overline{v}k$. Otherwise, when $\sum\limits_{j \in \mathscr{J}} (\overline{v} + w_j)k_j/q_j^0 > 1$, congestion takes place, and all vehicles will drive at a speed v less than \overline{v} . We will solve speed v as follows. At speed v, based on Eq. (7), we can obtain the corresponding pure traffic density for type-j vehicles as $\overline{k}_j(v) = q_j^0/(v + w_j)$. Given type-j vehicles density k_j , then we can obtain that the occupancy of type-j vehicles in the mixed traffic is $k_j/\overline{k}_j(v) = (v + w_j)k_j/q_j^0$. In congested traffic, the summation of the occupancies of all vehicle types should be identical to 100%, which yields

$$v = \frac{1 - \sum_{j \in \mathcal{J}} w_j k_j / q_j^0}{\sum_{j \in \mathcal{J}} k_j / q_j^0}.$$

The corresponding flow rate can be obtained as

$$q(k) = kv = \frac{1 - k \sum_{j \in \mathcal{J}} w_j \alpha_j / q_j^0}{\sum_{j \in \mathcal{J}} \alpha_j / q_j^0}.$$

Combining the results for both free-flow and congested regimes, we obtain the mixed traffic FD as

$$q(k) = \left\{ \frac{1 - k \sum_{j \in \mathcal{J}} w_j \alpha_j / q_j^0}{\sum_{k \in \mathcal{J}} \alpha_j / q_j^0}, \quad k \in \left[R, \frac{1}{\sum_{j \in \mathcal{J}} w_j \alpha_j / q_j^0} \right],$$

$$(8)$$

where
$$R=1/\Biggl(\sum\limits_{j\in\mathscr{J}}(\overline{v}+w_j)\alpha_j/q_j^0\Biggr)$$
.

Next, we illustrate how to apply the above formula with the pure FDs from dataset 1 (for the AV types) and dataset 3 (for the human-driven vehicle type). Fig. 9(a)-(d) show the FDs with different headway settings as the AV market penetration rate increases. It can be observed in Fig. 9(a) that as the AV market penetration rate increases, AVs with the shortest headway setting (headway 1)

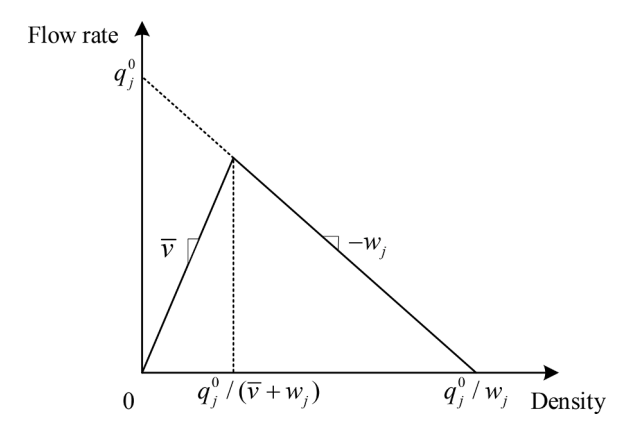


Fig. 8. Parameters illustration.

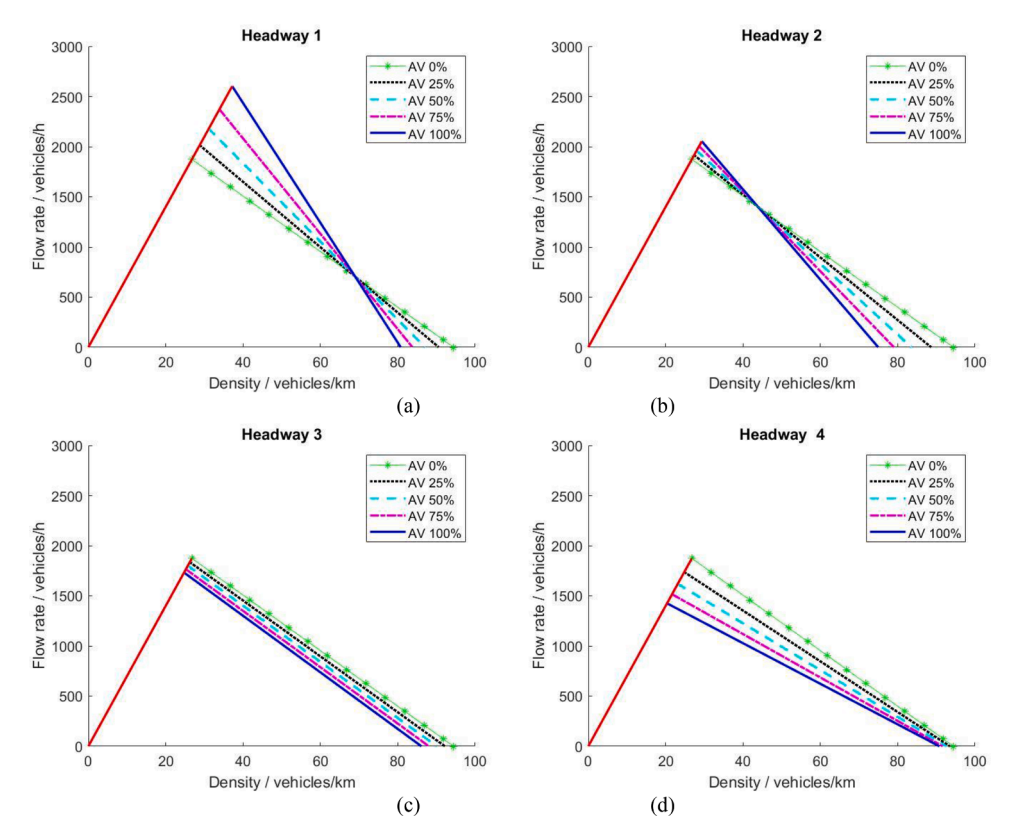


Fig. 9. FDs with different AV penetration rates and headway settings.

significantly improve the mixed traffic flow road capacity and shockwave speed, while the jam density does not change much. For the second shortest headway setting (headway 2) shown in Fig. 9(b), as the AV market penetration rate increases, the road capacity and shockwave speed slightly increase. Nevertheless, for headways 3 and 4 (Fig. 9(c) and (d)), the values of road capacity, shockwave speed, and jam density are found even smaller than that of human-driven vehicle traffic as the AV market penetration rate increases. These results further verify our findings that the results from the previous studies might be too optimistic to be applied to existing commercial AVs.

Together with the previous findings that a short headway setting can improve the traffic flow capacity at the cost of compromising traffic safety and stability, it is intriguing to appropriately manage the AV headway settings in future mixed traffic to balance the road capacity and traffic stability.

7. Conclusions and future research

Increasing the number of commercial AVs may lead to significantly different car-following behaviors compared with those of human-driven vehicles, which challenges the applicability of classic traffic flow theory. To help understand the impacts of commercial AVs on traffic flow, this paper proposed a general method that combines both empirical experiments and theoretical models to construct an FD for AV traffic. High-resolution trajectory data with multiple commercial AVs following one another in a platoon with different headway settings were collected to study the AV traffic flow characteristics. Data analysis results revealed that the traditional triangular FD structure remains applicable to describe the traffic flow characteristics of AV traffic. The comparisons and discussions among the FD results of AVs and human-driven vehicles indicated that though the shortest AV headway setting can significantly improve the road capacity, other headway settings may decrease the road capacity compared with existing human-driven-vehicle traffic. Further, this paper empirically verified that AV headway settings may affect the stability of the traffic flow. A mixed traffic FD construction approach was proposed to provide the basis for analysis, modeling, and simulation of future mixed traffic and draw managerial insights. The proposed general FD modeling approaches, which may be easily calibrated despite uncertainties and evolutions of the AV technologies, can serve as a methodological foundation for future mixed traffic flow studies.

This study can also be extended in the following directions. It would be interesting to verify the mixed traffic FD formula proposed in this paper by field experiment data with mixed-brands AVs and mixed headway settings. Moreover, the generated triangular FD alluded to issues such as the balance between traffic throughput and stability, which also raise the need to further investigate these issues from the perspective of management and policymaking. Also, it will be interesting to study the impacts of the connected vehicle technology and corresponding cooperative behaviors in conjunction with AVs on future mixed traffic performance.

Acknowledgments

This research is sponsored by Susan A. Bracken Faculty Fellowship and National Science Foundation Grants CMMI #1558887 and #1932452. Thanks for the efforts made by other members of the CATS lab in collecting the field experiment data, including Zhaohui Liang, Peng Zhang, Qianwen Li, and Handong Yao.

References

- Qian, Z., Li, J., Li, X., Zhang, M., Wang, H., 2017. Modeling heterogeneous traffic flow: a pragmatic approach. Transp. Res. Part B Methodol. 99, 183–204. https://doi.org/10.1016/j.trb.2017.01.011.
- Arnaout, G.M., Arnaout, J.P., 2014. Exploring the effects of cooperative adaptive cruise control on highway traffic flow using microscopic traffic simulation. Transp. Plan. Technol. 37, 186–199. https://doi.org/10.1080/03081060.2013.870791.
- Auld, J., Sokolov, V., Stephens, T.S., 2017. Analysis of the effects of connected-automated vehicle technologies on travel demand. Transp. Res. Rec. 2625, 1–8. https://doi.org/10.3141/2625-01.
- Auld, J., Verbas, O., Javanmardi, M., Rousseau, A., 2018. Impact of Privately-Owned Level 4 CAV Technologies on Travel Demand and Energy. Procedia Comput. Sci. 130, 914–919. https://doi.org/10.1016/j.procs.2018.04.089.
- Baskar, L.D., De Schutter, B., Hellendoorn, H., 2009. Optimal routing for intelligent vehicle highway systems using mixed integer linear programming. IFAC Proc. Vol. 42, 569–575. https://doi.org/10.3182/20090902-3-US-2007.0065.
- Bose, A., Ioannou, P., 2003. Mixed manual/semi-automated traffic: a macroscopic analysis. Transp. Res. Part C Emerg. Technol. 11, 439–462. https://doi.org/10.1016/j.trc.2002.04.001.
- Calvert, S.C., Schakel, W.J., van Lint, J.W.C., 2017. Will automated vehicles negatively impact traffic flow? J. Adv. Transp. 2017 https://doi.org/10.1155/2017/3082781
- Daganzo, C.F., 1997. Fundamentals of Transportation and Traffic Operations. Fundam. Transp. Traffic Oper. https://doi.org/10.1108/9780585475301.
- Daganzo, C.F., Geroliminis, N., 2008. An analytical approximation for the macroscopic fundamental diagram of urban traffic. Transp. Res. Part B Methodol. 42, 771–781. https://doi.org/10.1016/j.trb.2008.06.008.
- Delis, A.I., Nikolos, I.K., Papageorgiou, M., 2018. A macroscopic multi-lane traffic flow model for ACC/CACC traffic dynamics. Transp. Res. Rec. 2672, 178–192. https://doi.org/10.1177/0361198118786823.
- Edie, L.., 1963. Discussion of Traffic Stream Measurements and Definitions. 2nd Int. Symp. Theory Traffic Flow.
- Gayah, V.V., Gao, X., Nagle, A.S., 2014. On the impacts of locally adaptive signal control on urban network stability and the Macroscopic Fundamental Diagram. Transp. Res. Part B Methodol. 70, 255–268. https://doi.org/10.1016/j.trb.2014.09.010.
- Geroliminis, N., Sun, J., 2011a. Properties of a well-defined macroscopic fundamental diagram for urban traffic. Transp. Res. Part B Methodol. 45, 605–617. https://doi.org/10.1016/j.trb.2010.11.004.
- Geroliminis, N., Sun, J., 2011b. Hysteresis phenomena of a Macroscopic Fundamental Diagram in freeway networks. Transp. Res. Part A Policy Pract. 45, 966–979. https://doi.org/10.1016/j.tra.2011.04.004.
- (Sean) Ghiasi, A., Hussain, O., Qian, Z., Li, X., 2017. A mixed traffic capacity analysis and lane management model for connected automated vehicles: a Markov chain method. Transp. Res. Part B Methodol. 106, 266–292. https://doi.org/10.1016/j.trb.2017.09.022.
- Ghiasi, A., Li, X., Ma, J., 2019. A mixed traffic speed harmonization model with connected autonomous vehicles. Transp. Res. Part C Emerg. Technol. https://doi.org/10.1016/j.trc.2019.05.005.
- Greenberg, H., 1959. An Analysis of Traffic Flow. Oper. Res. 7, 79-85. https://doi.org/10.1287/opre.7.1.79.
- Gunter, G., Gloudemans, D., Stern, R.E., McQuade, S., Bhadani, R., Bunting, M., Monache, M.L.D., Lysecky, R., Seibold, B., Sprinkle, J., Piccoli, B., Work, D.B., 2020. Are Commercially Implemented Adaptive Cruise Control Systems String Stable? IEEE Trans. Intell. Transp. Syst. 19122, 1–12. https://doi.org/10.1109/TITS.2020.3000682.
- Gunter, G., Janssen, C., Barbour, W., Stern, R.E., Work, D.B., 2019. Model based string stability of adaptive cruise control systems using field data. IEEE Trans. Intell. Veh. 5, 90–99. https://doi.org/10.1109/TIV.2019.2955368.
- Knoop, V., Hoogendoorn, S., 2013. Empirics of a generalized macroscopic fundamental diagram for urban freeways. Transp. Res. Rec. 133–141. https://doi.org/10.3141/2391-13.
- Knoop, V.L., Daamen, W., 2017. Automatic fitting procedure for the fundamental diagram. Transp. B 5, 133–148. https://doi.org/10.1080/21680566.2016.1256239. Laval, J.A., 2011. Hysteresis in traffic flow revisited: an improved measurement method. Transp. Res. Part B Methodol. 45, 385–391. https://doi.org/10.1016/j. trb.2010.07.006.
- Levin, M.W., Boyles, S.D., 2016. A multiclass cell transmission model for shared human and autonomous vehicle roads. Transp. Res. Part C Emerg. Technol. 62, 103–116. https://doi.org/10.1016/j.trc.2015.10.005.
- (David) Liu, H., Kan, X., Shladover, S.E., Lu, X.Y., Ferlis, R.E., 2018. Modeling impacts of Cooperative Adaptive Cruise Control on mixed traffic flow in multi-lane freeway facilities. Transp. Res. Part C Emerg. Technol. 95, 261–279. https://doi.org/10.1016/j.trc.2018.07.027.
- Milanes, V., Shladover, S.E., Spring, J., Nowakowski, C., Kawazoe, H., Nakamura, M., 2014. Cooperative adaptive cruise control in real traffic situations. IEEE Trans. Intell. Transp. Syst. 15, 296–305. https://doi.org/10.1109/TITS.2013.2278494.
- Nagel, K., Schreckenberg, M., 1992. A cellular automaton model for freeway traffic. J. Phys. I. https://doi.org/10.1051/jp1:1992277.
- Newell, G.F., 1961. Nonlinear Effects in the Dynamics of Car Following. Oper. Res. 9, 209-229. https://doi.org/10.1287/opre.9.2.209.
- Nikolos, I.K., Delis, A.I., Papageorgiou, M., 2015. Macroscopic Modelling and Simulation of ACC and CACC Traffic. In: IEEE Conf. Intell. Transp. Syst. Proceedings, ITSC 2015-Octob, pp. 2129–2134. https://doi.org/10.1109/ITSC.2015.344.
- Qu, X., Wang, S., Zhang, J., 2015. On the fundamental diagram for freeway traffic: a novel calibration approach for single-regime models. Transp. Res. Part B Methodol. 73, 91–102. https://doi.org/10.1016/j.trb.2015.01.001.
- Qu, X., Zhang, J., Wang, S., 2017. On the stochastic fundamental diagram for freeway traffic: model development, analytical properties, validation, and extensive applications. Transp. Res. Part B Methodol. 104, 256–271. https://doi.org/10.1016/j.trb.2017.07.003.
- Robbins, C.J., Allen, H.A., Chapman, P., 2018. Comparing drivers' gap acceptance for cars and motorcycles at junctions using an adaptive staircase methodology. Transp. Res. Part F Traffic Psychol. Behav. 58, 944–954. https://doi.org/10.1016/j.trf.2018.07.023.
- Seo, T., Kawasaki, Y., Kusakabe, T., Asakura, Y., 2019. Fundamental diagram estimation by using trajectories of probe vehicles. Transp. Res. Part B Methodol. 122, 40–56. https://doi.org/10.1016/j.trb.2019.02.005.
- Shladover, S.E., Su, D., Lu, X.Y., 2012. Impacts of cooperative adaptive cruise control on freeway traffic flow. Transp. Res. Rec. 2324, 63–70. https://doi.org/10.3141/
- Soteropoulos, A., Berger, M., Ciari, F., 2019. Impacts of automated vehicles on travel behaviour and land use: an international review of modelling studies. Transp. Rev. 39, 29–49. https://doi.org/10.1080/01441647.2018.1523253.
- Tian, J.F., Yuan, Z.Z., Treiber, M., Jia, B., Zhang, W.Y., 2012. Cellular automaton model within the fundamental-diagram approach reproducing some findings of the three-phase theory. Phys. A Stat. Mech. its Appl. 391, 3129–3139. https://doi.org/10.1016/j.physa.2011.12.067.
- Van Arem, B., Van Driel, C.J.G., Visser, R., 2006. The impact of cooperative adaptive cruise control on traffic-flow characteristics. IEEE Trans. Intell. Transp. Syst. 7, 429–436. https://doi.org/10.1109/TITS.2006.884615.
- Wang, H., Ni, D., Chen, Q.-.Y., Li, J., 2013. Stochastic modeling of the equilibrium speed-density relationship. J. Adv. Transp. 47, 126–150. https://doi.org/10.1002/atr.172.

- Wang, Z., Shi, X., Li, X., 2019. Review of Lane-Changing Maneuvers of Connected and Automated Vehicles: models, Algorithms and Traffic Impact Analyses. J. Indian Inst. Sci. https://doi.org/10.1007/s41745-019-00127-7.
- Yao, Z., Hu, R., Wang, Y., Jiang, Y., Ran, B., Chen, Y., 2019. Stability analysis and the fundamental diagram for mixed connected automated and human-driven vehicles. Phys. A Stat. Mech. its Appl. 533, 121931 https://doi.org/10.1016/j.physa.2019.121931.
- Ye, L., Yamamoto, T., 2018. Modeling connected and autonomous vehicles in heterogeneous traffic flow. Phys. A Stat. Mech. its Appl. 490, 269–277. https://doi.org/10.1016/j.physa.2017.08.015.
- Zhang, J., Qu, X., Wang, S., 2018. Reproducible generation of experimental data sample for calibrating traffic flow fundamental diagram. Transp. Res. Part A Policy Pract. 111, 41–52. https://doi.org/10.1016/j.tra.2018.03.006.
- Zhou, J., Zhu, F., 2020. Modeling the fundamental diagram of mixed human-driven and connected automated vehicles. Transp. Res. Part C Emerg. Technol. 115, 102614 https://doi.org/10.1016/j.trc.2020.102614.
- Shi, X., Li, X., 2020. Empirical Study on Car Following Characteristics of Commercial Automated Vehicles with Different Headway Settings. Source: Preprint. https://doi.org/10.13140/RG.2.2.21464.32004/1.
- Li, X., 2020. Trade-off Between safety, Mobility and Stability in Automated Vehicle Following control: An analytical Method. Preprint https://www.researchgate.net/publication/343350105_Trade-off_between_safety_mobility_and_stability_in_automated_vehicle_following_control_An_analytical_method.
- Zhao, D., Shi, X., Yao, H., Li, X., Hale, D., Ghiasi, A., James, R., 2021. Video-based Trajectory Generation For High-Granularity Highway Simulation (HIGH-Sim). Preprint. https://doi.org/10.13140/RG.2.2.30725.06887.